Available online at www.sciencedirect.com

SCIENCE DIRECT®

EPSL

ELSEVIER

Earth and Planetary Science Letters 236 (2005) 285–304

www.elsevier.com/locate/epsl

The impact of precession changes on the Arctic climate during the last interglacial–glacial transition

Myriam Khodri [a,*], Mark A. Cane [a,1], George Kukla [a,2], Joyce Gavin [a,3], Pascale Braconnot [b,4]

[a] *Lamont-Doherty Earth Observatory of Columbia University, Palisades, NY 10964, USA*
[b] *Laboratoire des Sciences du Climat et de l'Environnement, 91191 Gif sur Yvette, France*

Received 6 October 2004; received in revised form 23 April 2005; accepted 4 May 2005
Available online 28 June 2005
Editor: E. Bard

Abstract

Three sensitivity experiments using an Ocean Atmosphere General Circulation Model (OAGCM) are conducted to simulate the climate impact of precession. The relative contributions of components of the hydrological cycle including the albedo of Arctic sea ice, advection of atmospheric water vapor and sea surface temperature to the summer Arctic melt process are evaluated. Timing of the perihelion is varied in each experiment with meteorological spring (SP), winter (WP) and autumn (AP) perihelion corresponding to conditions at 110, 115 and 120 ky BP, respectively. Obliquity is unchanged at the 115 ky level which is lower than today. The experiments are assessed relative to the present day control, which has been shown to simulate current conditions based on observations.

In the SP experiment, top of the atmosphere (TOA) insolation is weaker than today between the summer solstice and autumnal equinox. In the AP case representing the interglacial, it is less intense between vernal equinox and summer solstice but stronger during the remainder of the year. Although the incident solar radiation is reduced in summer in the SP experiment, increased melting of snow is found primarily as a result of feedbacks from the delayed seasonal cycle of hydrologic components. This is in contrast to both the WP and AP cases in which the perennial snow cover is simulated.

At the time of the last glacial inception, 115 ky BP, the WP experiment shows lower insolation to the high northern latitudes in late spring and summer mainly as a result of lower obliquity than today. Dynamical ocean–atmosphere interactions in response to precession maintain the reduced sea ice melting in late spring, strengthen the annual equator-to-pole sea surface temperature (SST) gradient and increase atmospheric moisture convergence in glaciation-sensitive regions. In both the WP and

* Corresponding author: Tel.: +1 845 365 8666; fax: +1 845 365 8736.
E-mail addresses: khodri@ldeo.columbia.edu (M. Kodri), mcane@ldeo.columbia.edu (M.A. Cane), kukla@ldeo.columbia.edu (G. Kukla), iceage@ldeo.columbia.edu (J. Gavin), Pascale.Braconnot@cea.fr (P. Braconnot).
[1] Tel.: +1 845 365 8344; fax: +1 845 365 8736.
[2] Tel.: +1 845 365 8421; fax: +1 845 365 8154.
[3] Tel.: +1 845 365 8416; fax: +1 845 365 8154.
[4] Tel.: +33 1 69 08 77 21; fax: +33 1 69 08 77 16.

0012-821X/$ - see front matter
doi:10.1016/j.epsl.2005.05.011

AP experiments seasonal sea ice melting is weakened resulting in pronounced outgoing radiative flux at the locations of expanded sea ice. This leads to further cooling and increased snowfall due to the reduced atmospheric water holding capacity and increased atmospheric moisture convergence from the subtropical Atlantic.

In agreement with Milankovitch theory, our results show favorable conditions for glacial inception at 115 ky BP but with obliquity unchanged, they also show perennial snow cover at 120 ky BP resulting from the reduced strength of spring insolation.

Keywords: glaciations; milankovitch; precession; insolation; Arctic Climate; Paleoclimatology; ocean/atmosphere interactions

1. Introduction

More than 150 years ago Adhémar [1] hypothesized a link between glaciations and the variation of earth's orbital parameters. He argued that the variation in precession, which controls the duration of the seasons with a periodicity of about 23,000 years, is the main mechanism accounting for glaciations by leading to longer winters in the Northern Hemisphere in contrast to the Southern Hemisphere. This theory had major caveats including the fact that it was known, from earlier work by d'Alembert (1717–1783), that each hemisphere receives exactly the same amount of insolation during the course of the year. Even though this fact invalidates Adhémar's theory, his idea that the total annual amount of insolation in high latitudes is important for the climate was new [for a detailed historical review the interested reader is referred to Bard [2]]. Since Croll [3] and then Milankovitch [4], who included eccentricity and obliquity, the cause of glaciations has been related to winter insolation and summer insolation, respectively. Milankovitch proposed that glacial inception occurs during periods of high eccentricity, low obliquity and winter perihelion. He reasoned that such an orbital configuration, which reduces northern summer insolation compared to present day in high latitudes, would prevent snowmelt in summer. Ice/snow albedo feedback would then lead to an ice age. The last period with this orbital configuration occurred ~115,000 years ago and according to radioisotopically dated deep-sea records [5,6], was indeed the beginning of the last glaciation.

The Milankovitch hypothesis of glaciation has been extensively tested with climate models ranging from conceptual models to coupled Ocean Atmosphere General Circulation Models (OAGCM) (e.g. [7–21]). The Atmospheric General Circulation Model (AGCM) experiments proved unable to simulate perennial snow cover over northern hemisphere lands under the insolation forcing of 115 ky BP (e.g. [21]). Vegetation feedbacks were shown to intensify the cooling of the northern high latitudes by way of increased surface albedo associated with the replacement of taiga by tundra. However, even the inclusion of vegetation-albedo feedbacks did not account for the establishment of perennial snow cover (e.g. [12]).

A study by Dong and Valdes [11] using a AGCM coupled to a mixed layer ocean shows that ocean surface–atmosphere interactions help to create favorable conditions of ice-sheet growth due to surface ocean cooling. Their model delivered perennial snow cover in regions thought to be the starting point of the ice sheets growth although the simulated summer cooling over high latitude oceans of 8 °C now appears unrealistic compared to marine data for this period. In their OAGCM experiment, Khodri et al. [13] have shown that perennial snow cover over northern Canada results from increased northward atmospheric moisture transport which brings more freshwater into the Arctic Ocean helping to extend the arctic sea ice cover, pushing the polar front southward [13–15] and cooling the local climate of the Canadian Archipelago enough to maintain perennial snow. These amplified moisture fluxes to the Arctic have since been simulated as a response to high-latitude perennial snow in an AGCM-only experiment that closely simulates the present climate over the Arctic [18,20]. Recent works on the MIS5e/5d transition using an Earth System Model of Intermediate Complexity (EMICs) show that the increase of arctic sea ice albedo from 126 to 115 ky BP almost doubled the northern high

latitudes summer cooling rate due to insolation changes, thus helping to create favorable conditions for glaciation [17,15]. However, all together, these findings still raise questions concerning the relative contribution and synergy of feedbacks between the major components of the hydrological cycle. Those which seem to be vital in the process leading to snow accumulation are the arctic sea ice albedo, the advection of atmospheric water vapor to northern high latitudes and the northern sea surface temperature (SST).

For the present day climate, the seasonal cycle of land snow cover and insolation are in quadrature (Fig. 1) mainly because of the time lag between

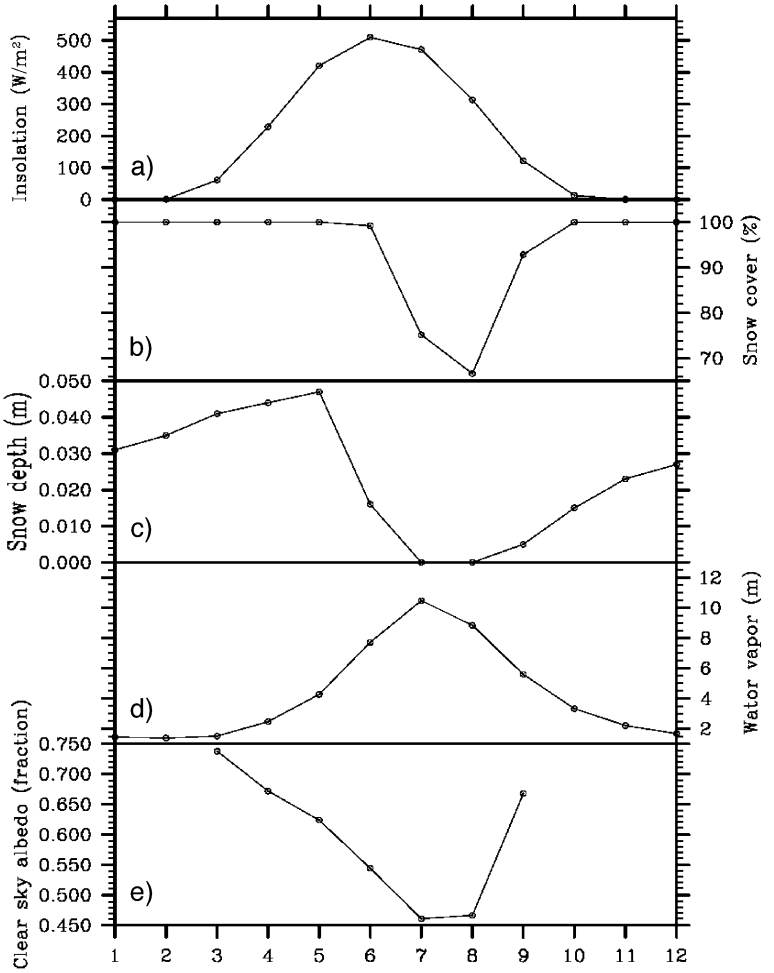

Fig. 1. Seasonal cycle of land snow cover and other variables over Northern Canada at (80° W, 80° N). (a) ERBE Solar incoming insolation (mean seasonal cycle 1985–1989, Lee and Barkstrom [46], (b) Snow cover from Northern Hemisphere EASE-Grid observations (mean seasonal cycle 1971–1995, Snowcover data provided by the NOAA-CIRES Climate Diagnostics Center, Boulder, Colorado, USA, from their Web site at: http://www.cdc.noaa.gov/), (c) Snow depth ECMWF Reanalysis-15 (mean seasonal cycle, 1979–1993, ECMWF Reanalysis-15 data provided by the NOAA-CIRES Climate Diagnostics Center, Boulder, Colorado, USA, from their Web site at: http://www.cdc.noaa.gov/), (d) Water Vapor NCEP/NCAR Reanalysis (mean seasonal cycle 1979–2001, Kalnay et al. [47]), (e) ERBE Clear sky albedo (mean seasonal cycle 1985–1989). Note that the discrepancy between snow cover and snow depth is probably due to the fact that the observations available for these two variables are not from the same dataset (one from EASE-Grid and the other from ECMWF) and do not cover exactly the same period: snow cover dataset covers a period ranging from 1971–1995 while the snow depth dataset covers a period ranging from 1979–1993. This figure helps illustrate the timing of seasonal changes of snow with respect to insolation income.

the major components of the hydrological cycle to the insolation change [22]. As shown in Fig. 1a–c, the snow cover in high northern latitudes is still fairly extensive in May despite the fact that the insolation received at the top of the atmosphere (TOA) is approaching its seasonal peak. However, at this time of the year, the surface ocean in mid to high latitudes is cold, sea ice cover is omnipresent, and the air is cold and dry. The incident solar radiation is high but the energy loss to space is also high due to the high surface albedo and the relatively low water vapor greenhouse effect (Fig. 1d–e). The net surface radiative budget stays low, allowing the snow cover to remain extensive until June. Snow melts only when the TOA insolation further decreases. In August all the snow is melting (Fig. 1b–c). The summer ablative environment in northern high latitudes is also influenced by water vapor greenhouse forcing and reduced surface albedo.

Milankovitch also evaluated the impact of insolation in Northern High latitudes at the ground where a critical element is the length of the passage of radiation through the atmosphere, which is exponentially longer with lower obliquity. At the time of the last glacial inception, 115 ky BP, the obliquity was lower respective to present day and the poles received less insolation over the year at the surface. Most of the reduction was taking place during late spring and summer while more energy reached low latitudes. Due to precession, the TOA insolation intensity increased between late autumn and early spring at the expense of late spring to early autumn (Fig. 2a). Given the lag between the seasonal changes of major components of the hydrological cycle and insolation forcing, it may be possible that insolation received during spring could potentially influence the atmospheric water vapor concentration and the surface albedo of the beginning summer (Fig. 1).

Was Adhémar totally wrong? What would be the consequences of a winter followed by reduced intensity of daily spring insolation? If perihelion was close to the autumnal equinox, the subsequent reduction of daily solar radiation received in spring could increase the summer season surface albedo, reduce water vapor greenhouse forcing and with it the surface energy budget. This question is even more relevant since most recent paleoclimatic data point to an important initial cooling of northern high latitude surface ocean [23–26] and land [27,28] between ~120 ky BP and 115 ky: a change which corresponds to the shift from autumnal to winter perihelion.

Most modeling studies focusing on the impact of the precession cycle mainly concern the response of tropical climate [29] to the combined effect of all orbital parameters or to precession alone [30,31]. Coupled ocean–atmosphere experiments [32] have shown that the response of the Asian monsoon strongly depends on the timing of the seasonal cycle of insolation. Crucifix and Loutre [17] using an EMICs have demonstrated through sensitivity studies that high latitude temperature changes during the last interglacial to glacial transition were mainly controlled by precession due to the growth of summer sea ice albedo feedback [33,20]. However, no modeling study published so far has explored the phase relationship of each component of the hydrological cycle to different precession configurations to evaluate their relative contribution to the local energy balance over northern high latitude land.

We investigated the above issue by comparing, in coupled ocean–atmosphere experiments, the climate response to three different precession configurations, corresponding to winter perihelion (WP) at 115 ky BP, autumnal perihelion (AP) at 120 ky BP and to spring perihelion (SP) at 110 ky BP. The present day control experiment serves as the basis of comparison. All three sensitivity experiments have lower obliquity compared to the control.

The model and experimental set-up are presented in Section 2. A brief discussion of the simulated modern day climate of high northern latitudes is also provided in this section. After describing the impact of the three precessional configurations on the seasonal cycle of northern high latitude snow cover and local energy balance all relative to the present day control experiment (Section 3), we examine the seasonal changes of arctic sea ice and freshwater budget (Section 4). We then focus on the seasonal variation of the atmospheric and oceanic northward heat transport and their relative contribution to the local energy balance over northern Canada (Section 5). In Section 6, the results are related to the Milankovitch theory and placed in the context of recent data and modeling studies of this period.

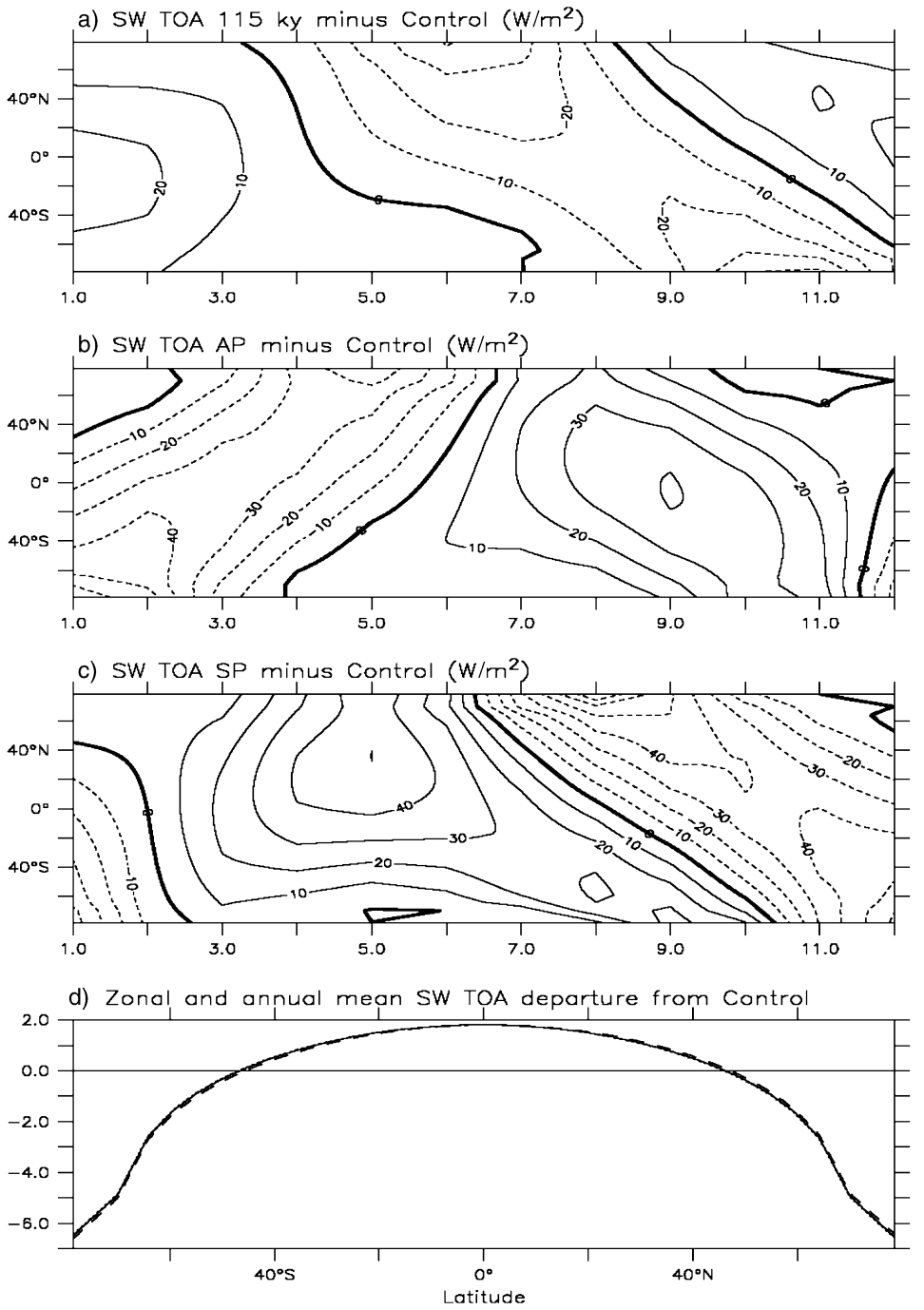

Fig. 2. Zonal mean difference of incoming solar radiation (W/m^2) at the top of the atmosphere (TOA) as a function of latitude and month between the control and (a) WP at 115 ky BP, (b) AP at 120 ky BP (c) SP at 110 ky BP. Contour intervals are every 10 W/m^2 with negative values as dotted lines. The annual zonal mean departure from the control of the TOA incoming solar radiation for each experiment is also shown (d) to illustrate that the three sensitivity experiments have exactly the same amplification of the equator-to-pole annual mean insolation gradient which reflects the obliquity which is lower than today.

2. Description of the model and experimental design

The following analyses are based in part, on the simulations of Braconnot and Marti [32] who utilized the IPSL-CM2 coupled ocean–atmosphere model [34,35] developed at the Institut Pierre Simon Laplace (IPSL, France), to study the mid-Holocene and present day monsoon system. Their experiments included two runs with all 115 ky BP orbital parameters but precession, fixed separately for autumn (AP) and spring (SP) perihelion corresponding to 120 and 110 ky BP, respectively. We ran the same model for a present day control run and for 115 ky BP climate corresponding to winter perihelion (WP). The atmospheric model has 50 grid points equally spaced in the sine of latitude and 64 points equally spaced in longitude. The atmospheric component includes a complex land-surface scheme [36]. The ocean component horizontal mesh is orthogonal and curvilinear on the sphere. The northern point of the convergence has been shifted onto Asia, in order to overcome the singularity at the North Pole. The ocean model's spatial resolution over high latitude reaches a maximum size of 4° by 3°. This version of the model includes a complex thermodynamic sea ice model with 3 different ice types with specific thermodynamic behavior [37]. The atmospheric and ocean model exchanges momentum, freshwater fluxes, sea ice concentration and albedo, and sea surface temperature once a day. The simulations are performed without flux corrections and are stable.

This version of the model has already been extensively used to study the present-day and mid-Holocene [32] monsoon system and the coupling between climate and the carbon cycle [38]. A discussion of the realism of the simulated modern day seasonal cycle is documented in previous analyses [34–39]. We address here the model in comparison to observations of the current hydrological cycle. The model has a low resolution, which allows us to perform longer simulations and test our hypotheses with various experimental configurations, without unduly sacrificing realism. While a higher resolution would be clearly preferable, our approach is a useful first step as suggested by three considerations. First, as can be seen by comparing Figs. 1, 4 and 5, the seasonal cycle of snow depth, atmospheric water vapor and clear sky albedo for the modern day control run (black solid line in Figs. 4, 5) compares fairly well with the observed seasonal cycle. In some places during winter over the Canadian Archipelago the snow depth is overestimated, but in the other respects the model does a good job in capturing the observed seasonal cycle, even quantitatively. This is in part related to the sub grid scale parameterization of the atmospheric boundary layer that distinguishes within a grid cell the various surface types [39]. Second, the error in annual land surface temperature of about 2 °C compared to a present day climatology [40] is considered to be small for state-of-the-art coupled models. Third, the sources of northern deep water are located in the Greenland–Iceland–Norwegian (GIN) seas where deep convection occurs in winter, allowing a deep-water flow through the Denmark Strait of about 6.1 Sv in close agreement with observed estimates of about 6 Sv [41]. Since most of the observed water exchange between the North Atlantic and the GIN seas (about 80%) is through the Denmark Strait, this is an important feature of northern high latitude-climate that is very well simulated. This feature is related to the realistic simulation of northern hemisphere sea ice cover and seasonal cycle [34]. The maximum (13.7×10^6 km^2) and minimum (7.5×10^6 km^2) ice extent, are close to satellites estimates (13.5 and 6×10^6 km^2, respectively).

The present day control run and the WP (115 ky BP) simulations are 120- and 100-years long, respectively. In the following analyses for the present day and the WP experiments, each are based on 70-year mean annual cycles. The AP (120 ky BP) and SP (110 ky BP) experiments were run for 50 years and we refer in the following to the last 30-years mean annual cycles. [32]. The present day control run serves as the basis of comparison. Table 1 summarizes the orbital parameters used in the control and the three preces-

Table 1
Orbital parameters of the Earth used for incoming solar radiation calculation at the top of the atmosphere [5]

	Control	WP	AP	SP
Eccentricity	0.016724	0.041421	0.041421	0.041421
Perihelion ($\omega - 180°$)	102.04°	110.88°	11°	219°
Obliquity	23.446	22.404	22.404	22.404

The position of the perihelion relative to the vernal equinox is measured by the ω angle. WP—winter perihelion; AP—autumn perihelion; SP—spring perihelion. In all simulations, the vernal equinox is set to 21 March at noon.

sion experiments. All three sensitivity experiments have the same obliquity, which is lower than that of the control.

For the WP case, the summer was longer but the associated mean daily insolation was weaker than present-day while in winter it was stronger (Fig. 2a). The change in the timing of perihelion in AP leads to stronger incoming solar radiation centered on the autumnal equinox (Fig. 2b) at the expense of the vernal equinox. The exact opposite situation occurs for SP (Fig. 2c). As shown in Fig. 2d, changes in the timing of precession have no impact on the annual mean TOA insolation. Only the lower obliquity compared to the control, is responsible for the annually amplified insolation gradient between low and high latitudes, which is shared by all three sensitivity experiments.

In Khodri et al. [13] we showed that for the present day OAGCM simulation, all the snow is melted over northern high latitude lands during summer. The WP (115 ky BP) has the same seasonal timing of precession and the reduced insolation during summer, (the present day ablation season) is caused by lower obliquity. The AP and SP simulations allow us to study the impact of the changing solar intensity during the transitional seasons.

3. Changes in the seasonal cycle of land snow cover over Northern Hemisphere high latitudes

Fig. 3a shows that the insolation difference of WP from the control run allows snow to last through summer [13]. In this experiment, where snow becomes perennial (80° W; 78° N), the June–July–August mean (referred to as summer season hereafter) of the TOA solar radiation decreases by about 27 W/m^2 while the net TOA solar forcing is reduced by close to 45 W/m^2 (Fig. 4a–b). It is surprising that despite the increased mean summer incoming TOA insolation (+4 W/m^2) in AP, the summer snow cover is more extensive than in the control or even in the WP experiment, going as far south as Newfoundland (Fig. 3b). More important, the snow is perennial over the Canadian Archipelago (98° W; 70° N), though the location is slightly different than in WP (Fig. 5a–c).

These results suggest that the planetary albedo must be larger in both the WP and AP runs. The difference between the TOA clear sky and non-clear sky net insolation (not shown) reveals a large reduction of the cloud radiative forcing (−78%) in WP, indicating that the surface albedo changes are responsible for the energy loss to space (+55%). This is confirmed by the pattern of the seasonal cycle of the atmospheric water vapor concentration and clear sky albedo shown in Fig. 4d–e. Since there is less net solar heating at the surface, the long wave radiation, latent and sensible heat must also change to bring the surface heating into balance; this requires a surface cooling of 9 °C in August (Fig. 4g–j). Consequently, the melting of snow during summer is reduced enough (Fig. 4k) to allow perennial land snow cover at high latitude of North America.

The autumnal perihelion in AP results in a lower water vapor concentration from May to August compared to the present day run (as expected from its characteristic 1-month lag behind insolation changes, Fig. 5d), generating a 29% mean summer reduction of the cloud radiative forcing. The clear sky albedo seasonal descent to its annual minimum is also delayed relative to the control, resulting in a 49% summer mean increase in surface albedo (Fig. 5e). The early seasonal reduction of TOA incoming insolation is responsible for the large net summer reduction of about 48 W/m^2 (Fig. 5a–b). The net heat budget reduction from late spring until midsummer accounts for a surface cooling of up to 10 °C in July (Fig. 5g–j) considerably limiting the snowmelt (Fig. 5k). Although the surface net heat budget during the following August to early fall is more positive, it is insufficient to get rid of the excess snow accumulation. The snowfall increases by 307% in July and, unlike the control, snowfall occurs in August (Fig. 5f). This latter result is rather counterintuitive since, as in the WP case, the atmosphere is drier during summer compared to the control (Fig. 4f). Examination of the atmospheric column shows that in both WP and AP, the summer cooling weakens the atmosphere's water holding capacity while increased moisture convergence from the subtropical Atlantic Ocean feeds high latitude snowfalls (Fig. 6). It is interesting to contrast the SP case with the AP one, which has only a seasonal shift in TOA insolation strength and yet presents almost the opposite scenario. The subtropical Atlantic moisture source in SP is reduced com-

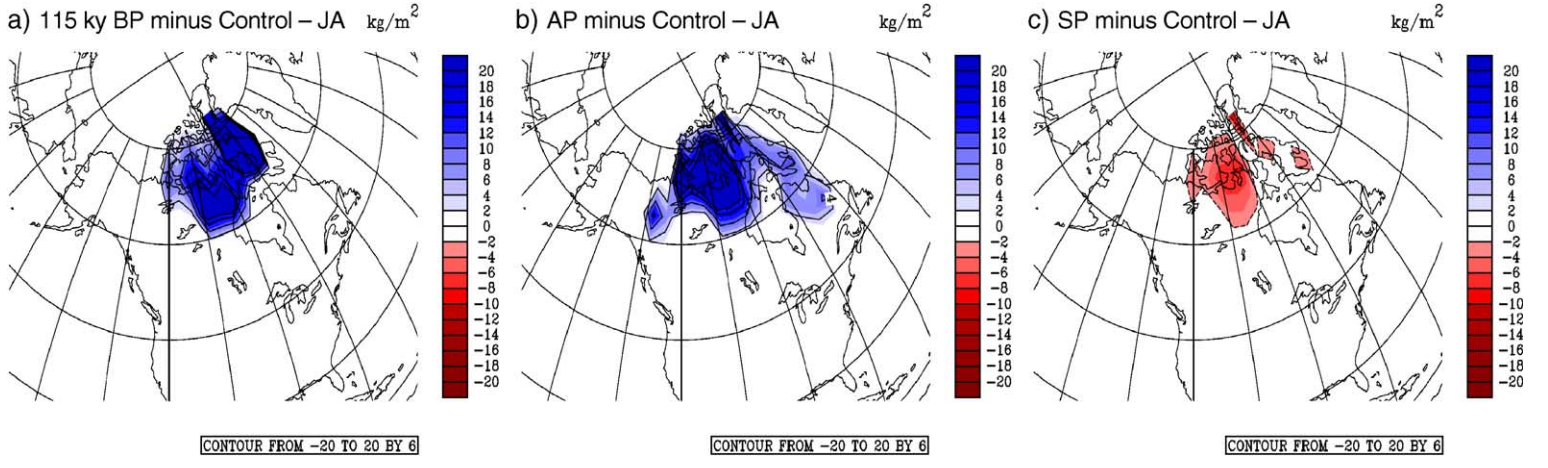

Fig. 3. July–August mean of snow depth (kg/m^2) over North America. Difference between the control for present day and (a) WP (115 ky BP), (b) AP (120 ky BP) (c) SP (110 ky BP). The shading indicates increased snow depth higher than 2 kg/m^2 and the hatchings a decrease stronger than -2 kg/m^2.

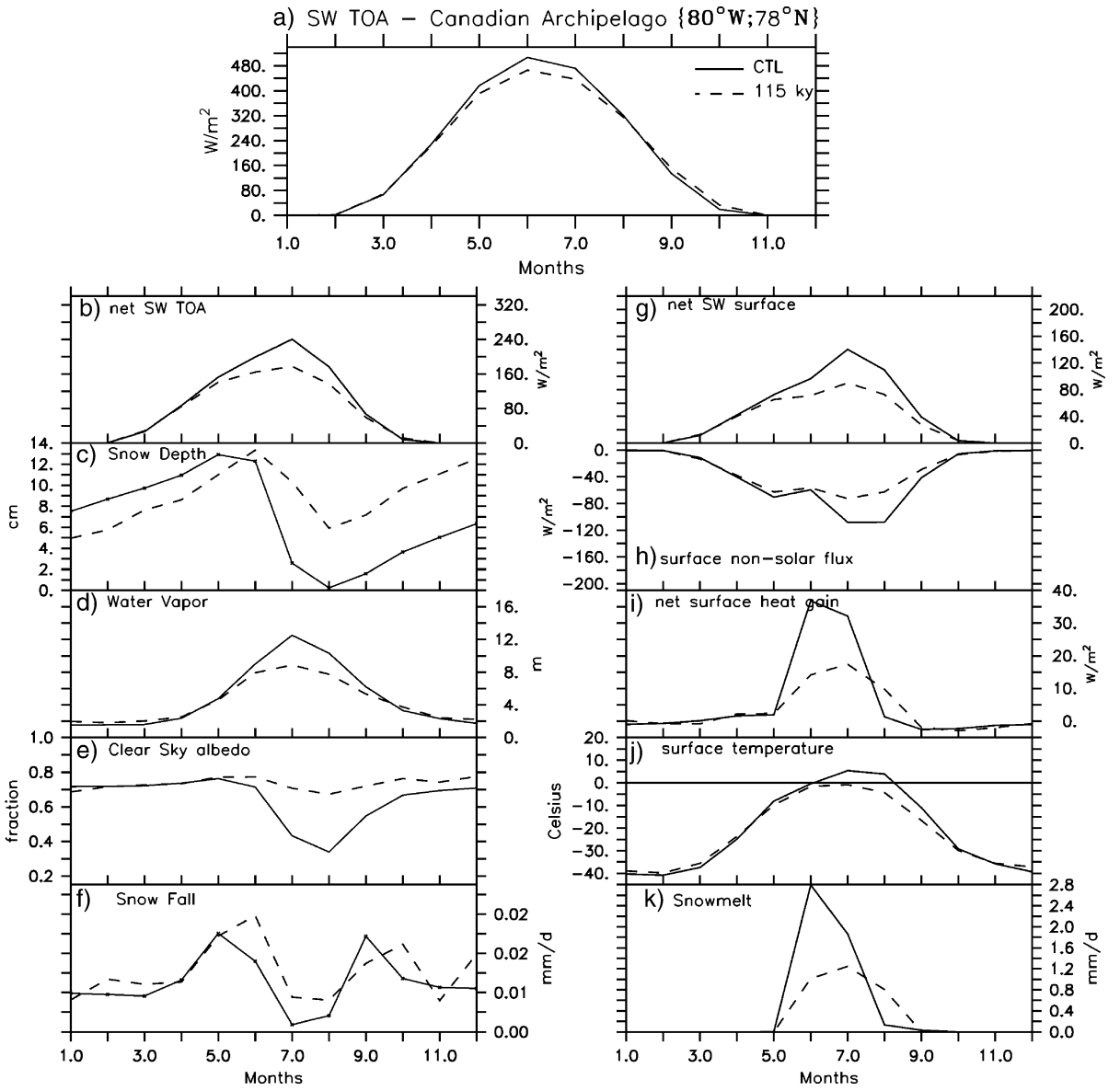

Fig. 4. Seasonal cycle of different variables contributing to the local energy balance and land snow cover over the Canadian Archipelago (80° W; 78° N). (a) Incident solar radiation at the top of the atmosphere (SW TOA) in W/m^2; (b) Net solar radiation at the top of the atmosphere (net SW TOA) in W/m^2; (c) Snow depth in cm; (d) Water vapor concentration in m; (e) Clear Sky albedo; (f) Snowfall in mm/day; (g) Net downward solar radiation at the surface in (net SW surface) in W/m^2; (h) Surface noon solar heat flux (including latent, sensible, and long wave radiation) in W/m^2, negative values indicate a heat loss for the surface; (i) Net surface heat gain (defined as the sum between the net SW surface and the non-solar heat flux) in W/m^2; (j) Surface temperature in °C; (k) Snowmelt rate in mm/day. On each panel, the black solid line stands for the present day control run and the dashed line for the WP (115 ky BP) simulation.

pared to both the WP and AP experiments, and so is the atmospheric moisture convergence over Northern Canada during summer (Fig. 6). The mean summer TOA incoming solar radiation decreases by 23 W/m^2 in SP compared to the control, but the summer snow cover over high latitudes of North America is considerably smaller (Figs. 3c, 6a–c). It appears that an early increase in solar forcing results in an early

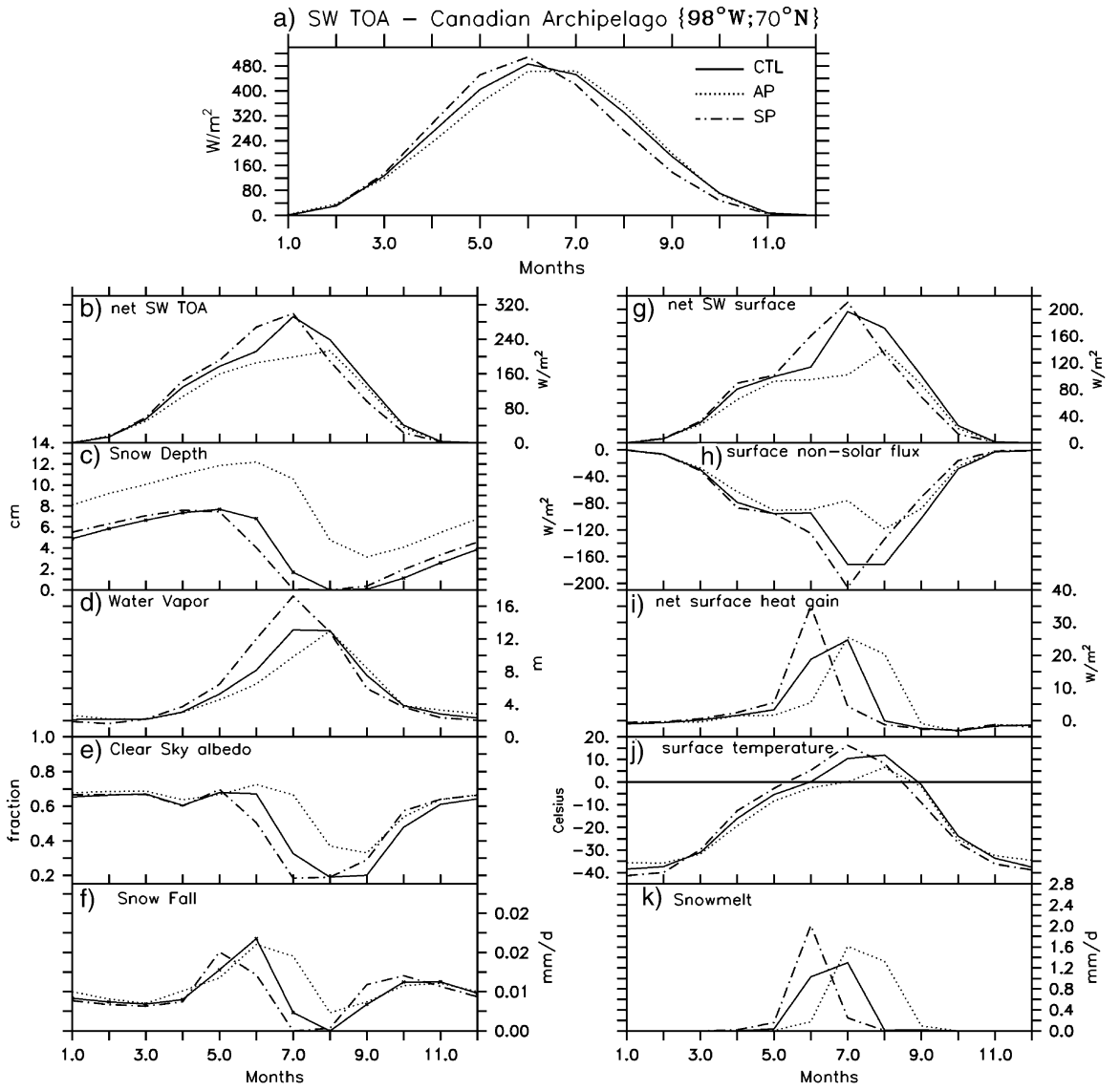

Fig. 5. Same as Fig. 4 but for an area located at (98° W; 70° N) in the Canadian Archipelago. The black solid line is for the present day control run, the dotted line for AP (120 ky BP) and the dashed-dotted line for SP (110 ky BP).

atmospheric moistening which is responsible for the opposite imbalance between the surface albedo (−25%) and cloud radiative forcing (+10%) (Fig. 5d–e) such that the net summer TOA insolation is slightly enhanced compared to the control (+6.2 W/m^2). The land surface warms (+6 °C in July), so upward surface heat fluxes increase (Fig. 5g–j). The net surface heat gain from April to June raises the snow-melting rate (Figs. 3d, 6c). There is more snowfall during fall (+35%) but it is too little and too late to compensate for the increased summer snow melting (Fig. 5f–k).

4. Changes in the seasonal cycle of Arctic Sea Ice

Analyses from different times (not shown) reveal that the changes of clear sky albedo responsible for

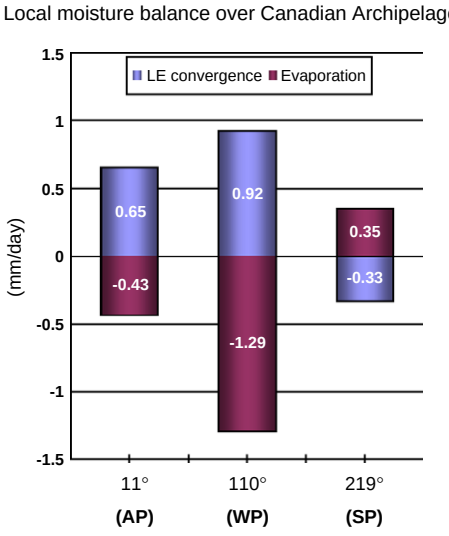

Fig. 6. July changes respective to the control of the Canadian Archipelago local moisture balance as a function of the perihelion longitude, including the contribution of the local evaporation and the moisture advection by atmospheric circulation. Units are mm/day.

the amplified loss of solar energy in the WP and AP and reduced loss in SP appear a few years before any snow accumulation (WP, AP) or melting (SP). Since the Canadian Archipelago is close to the Arctic Ocean, these clear sky albedo and cooling changes could be related to the changes of the Arctic sea ice seasonal cycle.

The critical times for the seasonal cycle of Arctic sea ice are the two pivotal seasons, spring when sea ice begins to melt and autumn when it starts to freeze (Fig. 7a–c,e). Because insolation reaching the Arctic surface during autumn is minimal (Fig. 7a), the sea ice freezing beginning in September is mainly related to the seawater temperature and salinity change (Fig. 7d,h). The relatively deep halocline in association with the surface ocean cooling facilitates the initial sea ice growth in September. Brine rejection then increases the seawater salinity until a maximum is reached in April (Fig. 7h). The melting beginning in April is strongly related to spring insolation, which first prevents surface water freezing at its southern-most margins. During the following summer the freshwater flux from sea ice controls the decrease in surface salinity of the Arctic Ocean. The contribution of precipitation minus evaporation is very small (Fig. 7e–g).

In the WP experiment in concert with the insolation forcing, the seasonal changes in arctic sea ice are similar to the changes in Canadian archipelago snow cover. However, sea ice reacts faster to the insolation than the snow cover; the summer sea ice melting is reduced prior to any changes in the clear sky albedo. The strengthening of the arctic halocline by an additional 15% annual river runoff into the Arctic Ocean reinforces this direct response to the summer insolation. The new equilibrium, reached after a 7 year long simulation, is then characterized by an annual mean increase in the sea ice pack by 50% and by the lowered amplitude of the sea ice mean seasonal cycle (Fig. 7a–c). As shown in Fig. 8, the additional sea ice expansion in summer north of the Greenland–Norwegian seas, Baffin Bay and north of North America, results in its surrounding of the region where the Canadian Archipelago's snow accumulates. Because the sea ice is already extensive in the autumn, less sea ice forms during winter and brine rejection is reduced (Fig. 7f). The limited winter brine rejection, together with the somewhat weaker summer melting, produce a reduced amplitude in the Arctic surface salinity seasonal cycle (Fig. 7f–h). The surface waters are also colder in the Arctic Ocean due to the enhanced insulating effect of sea ice cover (Fig. 7d).

The AP experiment presents almost the same changes in sea ice characteristics as the WP simulation, but here it is the delayed spring melting which gives a higher annual mean pack ice at the equilibrium (+33%; Fig. 7a–d). The annual mean river runoff increases by about 18%, helping sea ice to expand in summer to the same area as in WP but with a higher mean concentration (Fig. 8). Thus, although the mean August–September melting rate is twice as strong as in the control (2.5 times higher than in the WP experiment), it is not enough to get rid of the excess sea ice maintained during summer (Fig. 7b–c,f). The cooling is larger all year-long in AP than in WP due to additional sea ice cover during spring and the beginning of summer (Fig. 7d). Conversely, in SP, due to the low dependency of sea ice freezing on autumn insolation, the solar forcing decrease in the autumn does not compensate for the summer melting, which starts earlier in the year (Fig. 7f). This is confirmed by the sea surface salinity values during autumn, which increase as the sea ice pack does, but never reach the

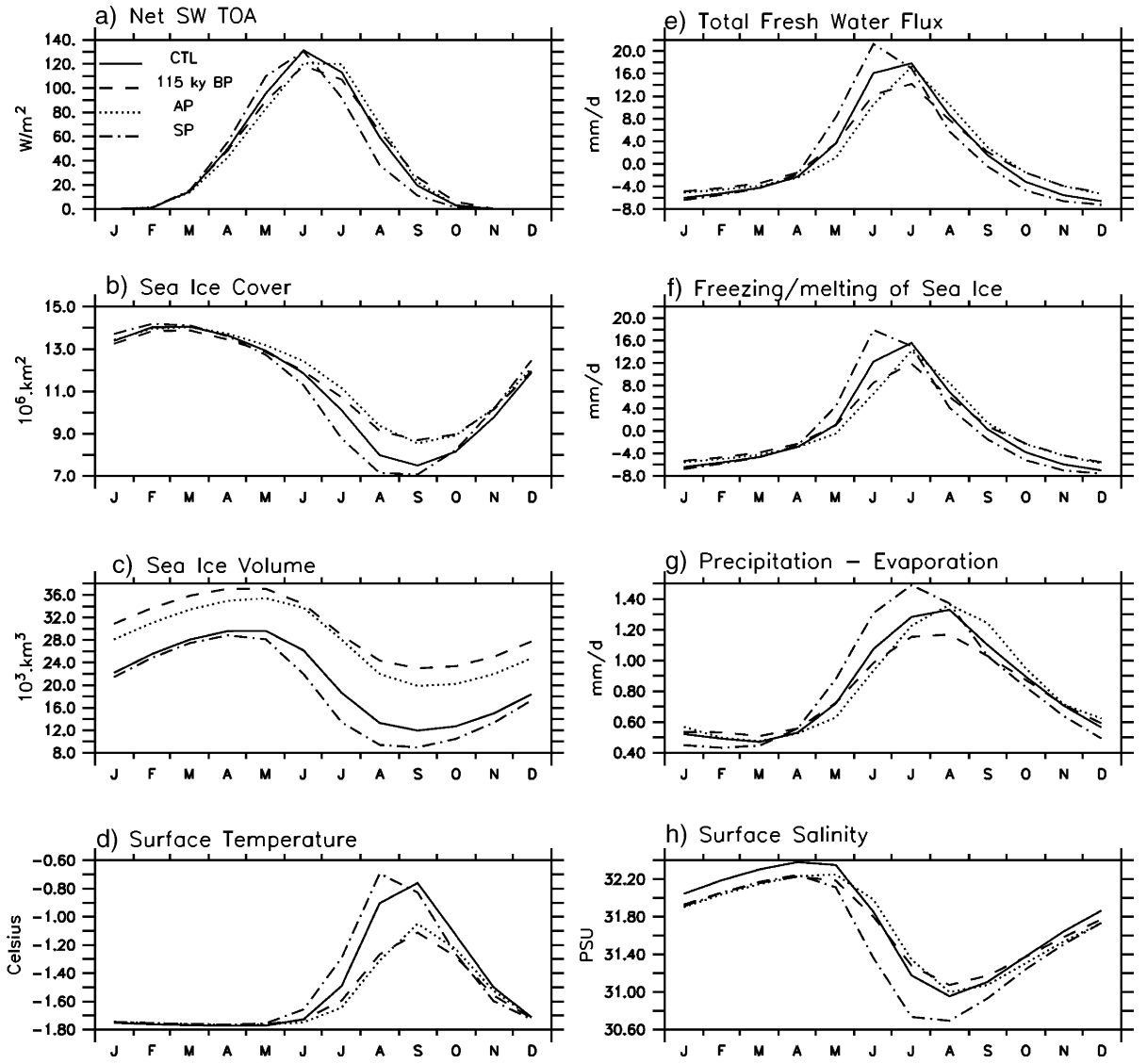

Fig. 7. Seasonal cycle of insolation, sea ice, surface salinity and temperature in Arctic Ocean. (a) Net incident solar radiation at the top of the atmosphere over Arctic Ocean (net SW TOA) in W/m^2; (b) Sea ice cover in 10^6 km^2; (c) Sea ice volume 10^3 km^3; (d) Surface temperature in °C; (e) Total freshwater flux at the ocean surface; (f) Freshwater flux to the ocean due to sea ice freezing and melting. Negative values indicated sea ice formation which uptake freshwater from the ocean while positive values indicate melting and therefore freshwater flux to the ocean; (g) Precipitation minus evaporation; from (e) to (g) units are mm/day; (h) Surface salinity in PSU. The black solid lines represent the control run, the dashed lines for the WP (115 ky BP) experiment, the dotted lines for AP (120 ky BP) and the dashed-dotted lines for SP (110 ky BP).

control values. As in the other sensitivity experiments (Fig. 7h), the annual mean salinity is reduced, but here this change is not accounted for by the runoff changes but by the enhanced spring sea ice melting. The summer sea ice concentration is reduced precisely where in the AP and WP experiments sea ice concentration increases (Fig. 8), illustrating the great dependency of the sea ice physical properties on spring insolation. At equilibrium, the mean arctic ice pack decreases by about 10% and the mean amplitude of

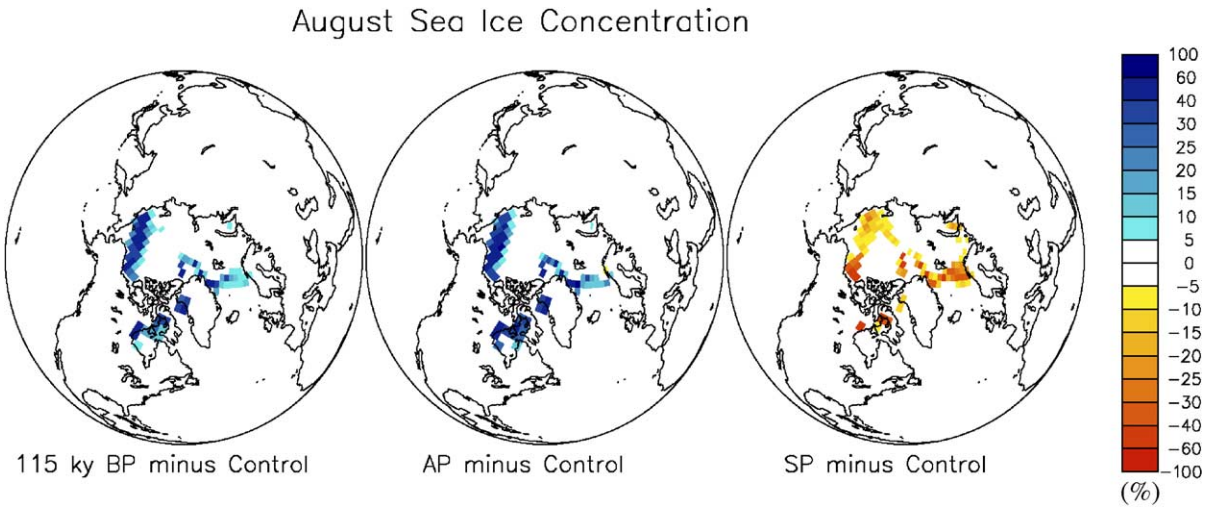

Fig. 8. August changes of sea ice concentration in Arctic Ocean (in percent) for each sensitivity experiment respective to the control.

the seasonal cycle of both sea ice cover and volume is enhanced (Fig. 7b–c).

From these results, it is obvious that through its albedo, the changes in the Arctic sea ice mean seasonal cycle play a central role in the local energy budget over regions where snow accumulates in WP and AP and melts in SP. Such rapid changes in sea ice physical properties must also impact the ocean and atmospheric circulation and in turn their contribution to the processes occurring in Arctic and over the Canadian Archipelagoes.

5. Changes in atmosphere and ocean circulation

At a given latitude, the precession parameter modifies the seasonal cycle of insolation without changing the annual mean TOA insolation. On the other hand, the lowered obliquity relative to the present, shared by the three sensitivity experiments, induces the same increased annual mean equator-to-pole insolation gradient (Fig. 2d). Because of this, the total northward heat transport has to increase. By breaking down the total northward heat transport between the atmosphere (Fig. 9) and the ocean contribution (Fig. 10), two features immediately stand out: in WP and AP, the heat deficit in the high latitudes is balanced by a significant northward atmospheric heat transport mainly as latent heat while in SP the lion's share of the response comes from the ocean heat transport (OHT). Two mechanisms explain the differences between the early and the late insolation forcing.

The first is the seasonal changes of the principal control of moisture availability for the atmosphere, which is the state of the ocean surface. The seasonal change in ocean surface temperatures is controlled by insolation [42]. Because of the ocean heat capacity, sea surface temperatures lag behind the insolation by 2–3 months. Therefore, in both the WP and AP experiments, the insolation forcing acts to cool North Atlantic high latitudes while warming the tropical Atlantic. A seasonal breakdown of the SST anomalies reveals that this results from a larger SST gradient between summer and autumn in WP and between spring and summer in AP, which accounts for all the increase in northward moisture advection (Fig. 9 a–b), more precipitation over northern hemisphere lands and more Arctic river runoff. In SP, on the other hand, the larger SST gradient during early autumn leads to more northward moisture advection and is almost canceled by the reversed situation during late spring. As a result, the annual mean is not changed significantly (Fig. 9c). We conclude that the ocean surface thermal response to the winter/autumn perihelion translates

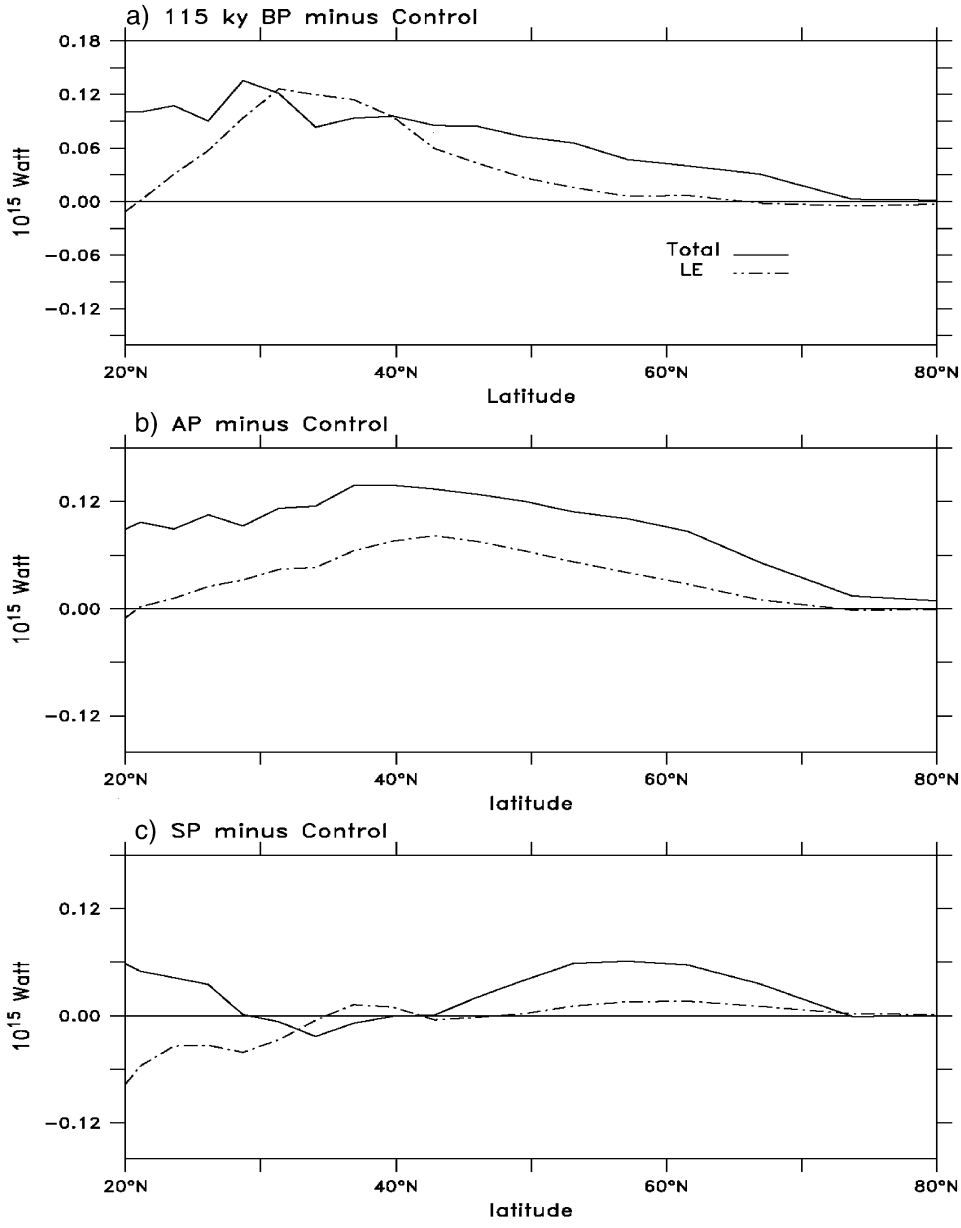

Fig. 9. Annual mean change respective to the control of atmospheric heat transport north to 20° North for (a) WP—115 ky BP, (b) AP–120 ky BP and (c) SP–110 ky BP. The black solid line represents total atmospheric heat transport (total) and the dashed dotted line the latent heat (LE) component. Positive values indicate increased northward transport.

into an increase of annual northward moisture transport, thus amplifying the changes due to obliquity. Conversely, spring perihelion damps the obliquity effect on the atmospheric circulation but allows the OHT to take over.

The second mechanism is related to the combined impact of changes in the arctic freshwater budget and atmospheric forcing on ocean surface circulation. During winter in the WP and AP cases, the 2–3 °C warming of the Northern Hemisphere land generates

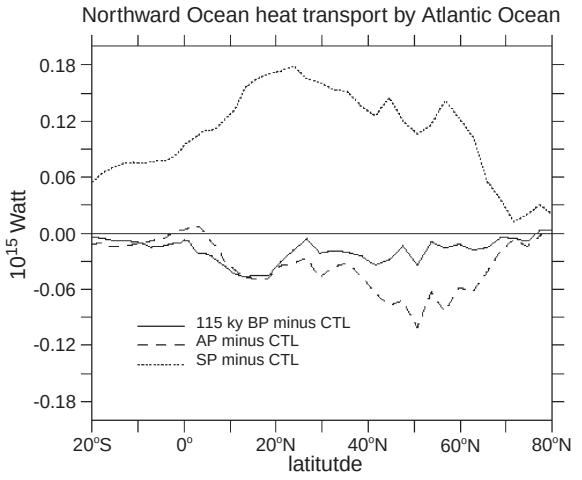

Fig. 10. Annual mean change respective to the present day control of the zonally and vertically integrated northward ocean heat transport over the first 500 m in the North Atlantic (in PW) for WP (115 ky BP) black solid line; AP (120 ky BP) dashed line; and SP (110 ky BP) dotted line.

an anomalously weak pressure system over northern continents and northern Greenland, reducing the anticyclonic flow and associated Ekman convergence in the ocean. More Arctic water can therefore expand southward along the Greenland coast, which cools North Atlantic SST as far as 60° N in WP and 40° N in AP (Fig. 11a–c). This advected colder water, together with the insolation-forced warming of lower latitudes, weakens the pressure gradient between the Iceland Low and the Subtropical Atlantic High and with it the surface wind stress. The anomalous northeasterlies over the Atlantic western-boundary effectively damp the northeastward ocean heat advection. These results suggest that the prevailing wind anomalies and the lower arctic salinity work together to reduce 0.45 Sv (WP) and 0.56 Sv (AP) to the thermohaline outflow through the Denmark Strait while reducing the water import through the Iceland–Scotland ridge by 0.16 Sv (Fig. 12). In SP, changes in the land surface temperature over the Northern Hemisphere are small and here the reduced anticyclonic circulation over the Arctic Ocean is due to the warmer mid-to-high latitude oceans (Fig. 11d–h). But the expansion of the arctic waters along the eastern Greenland coast is blocked by the reinforced wind driven ocean circulation in the western boundary of North Atlantic (not shown). In SP, in contrast to WP/AP, both the changes in thermohaline and wind-driven forcing lead to more water mass exchanges through the Greenland–Iceland–Scotland ridge (Fig. 12) reflecting the northward shift of the polar front.

Interestingly, the changes in the northward ocean heat transport simulated during winter are maintained during the summer season, but not for the same reason. In both the WP and AP experiments, high pressure builds up over Northern Hemisphere continents due to cooler lands. But, in WP, the warmer tropical ocean weakens the subtropical Atlantic anticyclonic circulation and consequently the North Atlantic Drift. In the AP case however, the Arctic water advected along the Atlantic western boundary down to 40° N during winter is still present (Fig. 11g). The cold water is responsible for the anomalous cyclonic circulation over the mid-Atlantic, which elicits a southward shift of the zero line of the wind stress curl and a rerouting of the North Atlantic Drift off the coast of Portugal instead of to higher latitudes. In SP, the opposite situation occurs and leads to reinforced wind-driven circulation over the western Atlantic boundary as in winter.

We may conclude that the winter and autumn perihelion in WP/AP amplifies the obliquity impact on the North Atlantic SST gradient, which helps to increase the northward latent heat transport. The Arctic surface waters are freshened by the subsequent increased runoff. The precession changes in these experiments also reduce the surface wind stress throughout the year over the western boundary of the North Atlantic and together with the less salty arctic water leads to a reduced OHT. In the SP case, the induced annual increase of atmospheric heat transport by the obliquity change is almost canceled by the spring perihelion. Although the surface arctic waters are fresher due to higher sea ice melting, the precession amplifies the ocean circulation and tips the balance of the increased northward heat transport in favor of the ocean. Several other studies have shown that lower obliquity alone acts to reduce the net TOA radiation balance in high latitudes during late spring and early summer [20,22]. According to our result however, this feature would be canceled by the changed timing of perihelion.

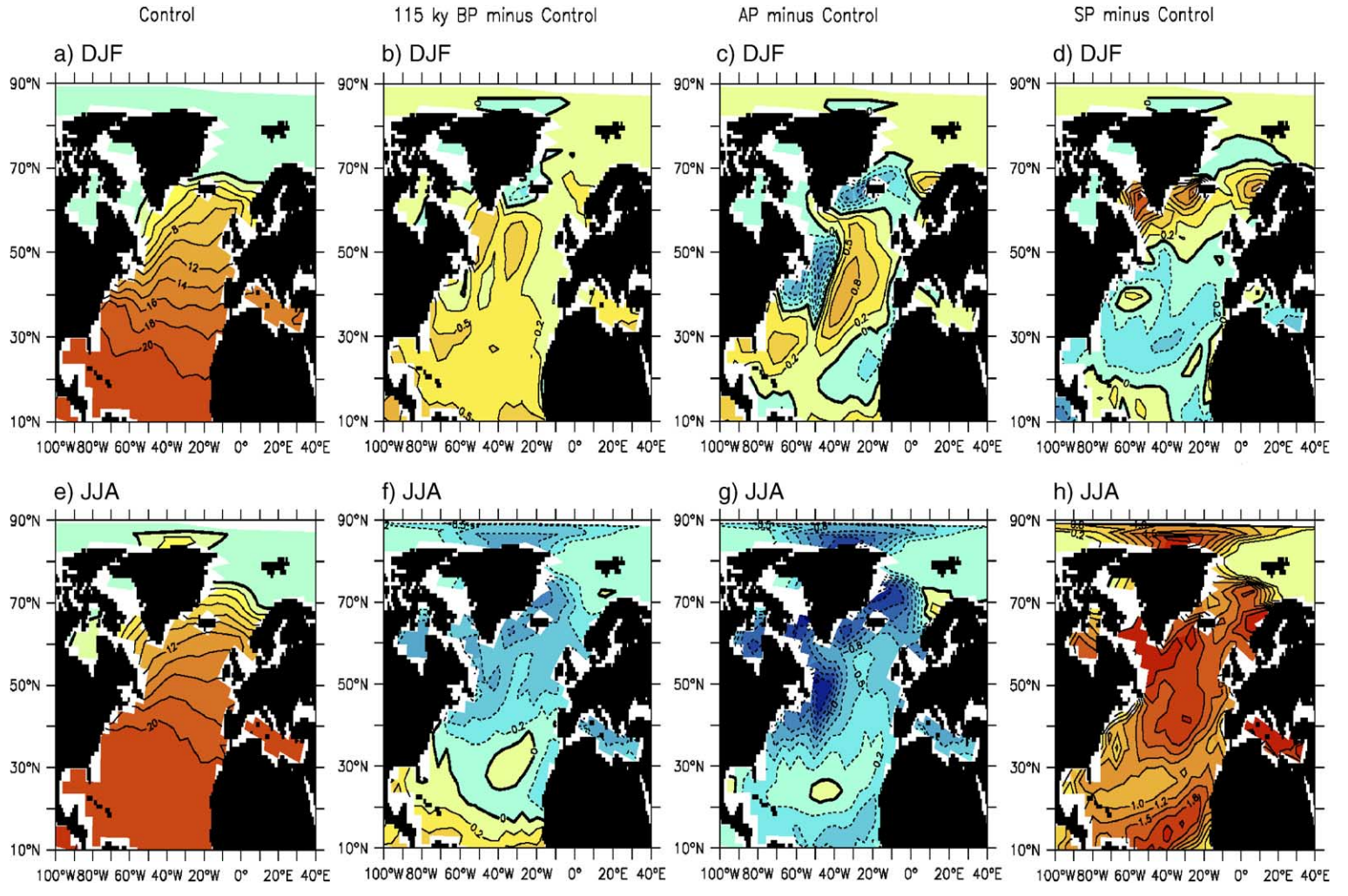

Fig. 11. Sea surface temperature (°C) over the North Atlantic Ocean. (a) for the control in December–January–February (DJF), and (e) June–July–August mean (JJA); (b) departure from the control for the WP (115 ky BP) for DJF and (f) JJA; (c) departure from the control for AP (120 ky BP) in DJF and (g) JJA; (d) departure from the control for SP (110 ky BP) in DJF and (h) JJA. In (a) and (e) contour intervals are every 2 °C. In (b) to (d) and (f) to (h) the contour intervals are every 0.2 °C.

6. Discussion and conclusion

We have shown that snow cover over the Canadian Archipelago becomes perennial in both the WP and AP experiments while the snow melting is amplified in the SP case. The sign of the feedbacks from each component of the hydrological cycle depends on the seasonal phasing of insolation; a shift of perihelion to winter or autumn amplifies the solar change due to obliquity while a shift to spring counteracts it.

In GCMs, as in nature, the net surface heat gain in summer is used to increase land snow temperature up to the freezing point, and then the excess energy is used to melt the snow. Experiments with AGCMs or AGCMs coupled to vegetation models, needed a summer cooling of 10 °C compared to the present day to prevent the summer snow from melting away [9,11,12,30]. Here, with an OAGCM, we have shown that due to the low obliquity of 115 ky BP in association with both winter and autumn perihelion, the land surface heating could be reduced enough to maintain the snow during summer; the cooling reaches the critical value of 10 °C. With spring perihelion however, despite the reduced summer TOA insolation, the opposite effect results. A new sea ice equilibrium is reached after 7 years of simulation (Section 4) in which Arctic sea ice expands on its southern and western margins in the WP/AP experiments while the melting is increased over the same areas in the SP case. Land temperatures are also expected to equilibrate quite fast to an insolation anomaly and yet the snow melting in the Canadian Archipelagos is not reduced until sea ice spreads to their coasts and increases the surface albedo locally. Afterwards, the summer surface energy budget is significantly reduced and summer land temperature stays below zero. Present day observations show that in winter a high-pressure system dominates the Arctic with cold, dry arctic air transferred southward in frequent polar air outbreaks. From our results it is conceivable that during the last glacial inception these processes could have also occurred in summer, amplifying the inland cooling due initially to reduced local insolation income. In our experiments it appears that the more the sea ice expands toward the Canadian Archipelagos, the cooler and drier the overlying atmosphere becomes. As for the Milankovitch theory, it appears that before the snow can accumulate and generate an albedo feedback, it is necessary to trigger the albedo effect by growing Arctic sea ice. However, in order to quantify the snow–sea ice interactions, future sensitivity experiments should be performed.

The contribution of the atmosphere is far from negligible. The changes in the prevailing winds and northward atmospheric moisture transport appear to be the cornerstone of the simulated snow accumulation over high latitudes of North America. The op-

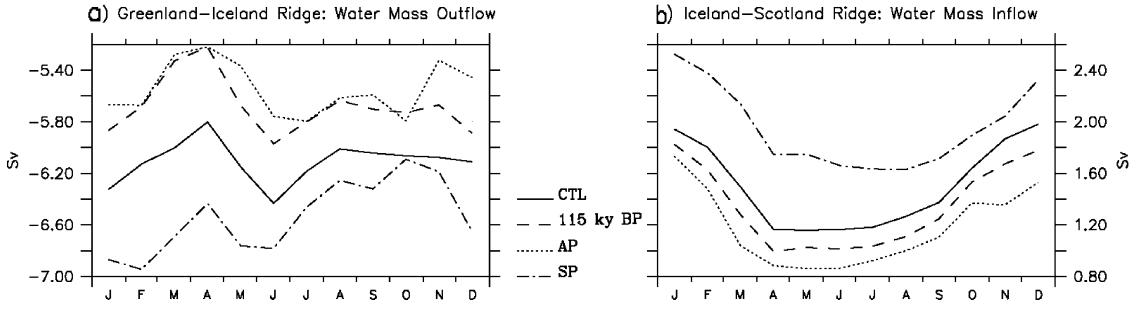

Fig. 12. Seasonal cycle of water inflow and outflow from the Arctic Ocean through the Greenland–Iceland–Scotland Ridge. (a) Vertically integrated water mass export from Arctic through the Greenland–Iceland Ridge (Sverdrup), (b) Vertically integrated water mass import from the Atlantic through the Iceland–Scotland (Sverdrup). The black solid curve represents the present day control, the dashed curve for WP (115 ky BP), the dotted curve for AP (120 ky BP) and the dashed-dotted curve for SP (110 ky BP). In (a) and (b), negative value indicates a southward water mass transport and positive values a northward mass transport. For the WP and AP experiments, the winter water mass export through the Greenland–Iceland Ridge is reduced by about 0.45 and 0.56 Sverdrup (Sv) respective to the control while the water import through the Iceland–Scotland Ridge is decreased by about 0.16 Sv in both experiments. SP water mass export through the Greenland–Iceland Ridge from the Arctic is amplified by about 0.68 Sv and the import of water from the North Atlantic through the Iceland–Scotland Ridge increased by 0.59 Sv.

posite response of the atmospheric circulation to a winter or autumn perihelion timing and to a spring perihelion leads to almost the opposite chain of feedbacks (see Table 2). They can be summarized as follows:

(1) The Arctic Sea Ice. With a winter or autumn (spring) perihelion, the increased (decreased) northward moisture transport by the atmosphere leads to an increased (unchanged) annual mean runoff into the Arctic. Combined with the precession impact it influences sea ice characteristics. Strengthening of the halocline with the decreased (increased) spring insolation work to enhance (reduce) the mean sea ice volume and expansion.
(2) The Ocean Circulation. Our OACGM simulations are too short to address the impact of precession on the deep ocean circulation, but are long enough to discuss the impact on the thermohaline water outflow through the Denmark Strait, surface salinity-mixed layer depth over the GIN Seas and the position of the polar front. The mid-latitude atmospheric wind stress in the North Atlantic is damped (amplified) with a winter or autumn (spring) perihelion. The associated changes in transports at high latitudes push the position of the polar front southward (northward) throughout the year leading to fresher and colder (saltier and warmer) subpolar North Atlantic Water and reduced (increased) winter mixed layer depth. Thus with a winter or autumn perihelion the ocean surface is able to translate the seasonal insolation anomalies due to precession into an annual signal, amplifying the increased SST gradient due initially to the lower obliquity. The spring perihelion (SP), on the other hand, almost cancels the obliquity effect on atmospheric heat transport, favoring oceanic heat transport.
(3) The Snow Cover. The annual northward latent heat convergence over the Canadian Archipelago increases in response to the progression of the perihelion from autumn (120 ky BP) to winter (115 ky BP), principally because of phase locking with the obliquity impact on the SST gradient (Fig. 6). The change in the atmospheric moisture transport from the tropics toward high latitudes helps to bring more (less) moisture over the Canadian archipelago. Together with the reduction (increase) of atmospheric water holding capacity arising from the increased (reduced) high latitude cooling generated by the two previous feedbacks, an increased (reduced) snowfall results.

Table 2
Impact of precession on the northern high latitude climate: summary of the main changes compared to the control run in percent

Changes compared to the control run (%)	WP	AP	SP
Summer SW TOA over Canadian Archipelago	−6.0	+1.0	−5.0
Summer NET SW TOA over Canadian Archipelago	−22.2	−19.6	+1.6
Summer atmospheric water vapor concentration over Canadian Archipelago	−22.6	−15.7	+22.7
Summer clear sky albedo over Canadian Archipelago	+55.0	+49.0	−25.0
Summer Arctic Sea ice volume	+51.0	+44.0	−23.0
Summer atmospheric moisture convergence over Canadian Archipelago	+1533.0	+176.0	−90.0
Annual northern equator-pole SST gradient	+5.0	+4.4	−4.0
Annual northward ocean heat transport	−6.0	−16.0	+26.0

Designations as in Table 1.

According to SST data inferred from marine cores in the North Atlantic Ocean and our model, the high latitudes experience a cooling reaching a maximum around 120 ky BP (autumn perihelion), followed by another cooling step at 115 ky BP (winter perihelion), both events being associated with low salinity values in the Northern Seas and a significant shallowing of North Atlantic Deep Water [23–26,43–45]. From our results it appears that those changes are due to the impact on the hydrological cycle responding to the perihelion shift from autumn to winter, probably also amplified by the decreasing obliquity during this time period. Our results support the idea that precession has a strong hold on the northern high latitude climate through the sea ice albedo feedback [17,33,15]. Our work indicates that sea ice albedo helps not only to reduce the snowmelt but also to reduce the water holding capacity of the atmospheric column and in-

crease snowfall. Ocean–atmosphere interactions in response to precession changes also amplify the obliquity related increased equator-to-pole SST gradient and moisture convergence into glaciation sensitive regions. Vettoretti and Peltier [19] have also shown that, if the control climate is unbiased, perennial snow cover can be simulated in AGCM-only experiments, leading to an amplification of the northward moisture convergence. According to the authors, the sole impact of the decreasing obliquity is to reduce northern high latitude insolation mainly during late spring [20], which, according to our results, may work in concert with the precession to explain the observed chronology of events from 120 to 110 ky BP over the ocean. These findings show that the increased surface albedo necessary to trigger glacial inception could have potentially operated as early as 120 ky BP, due to the impact of the reduced spring insolation on sea ice. In conclusion, in agreement with Milankovitch theory, our results show that 115 ky BP orbital configuration is favorable for glaciations, but as suspected by Adhemar (1842), a winter climate aided by a cold spring (AP) could have prepared as early as 120 ky BP, a transition of the Earth's climate into the last Ice Age.

Acknowledgements

Support was provided by grant UCSIO CU (02165401 SCF) of the NOAA ARCHES program and by NSF grant ATM-04-45038. The simulations were performed on the VPP5000 of the Comissariat à l'Energie Atomique (France). We would like to thank two anonymous reviewers and the Editor for their useful comments that helped us improve the quality of this manuscript. This is a Lamont Doherty Earth Observatory contribution 6767.

References

[1] J.A. Adhémar, Révolutions de la Mer: Déluges Périodiques, Carilian-Goeury et Victor Dalmont, Paris, 1842, 184 pp.
[2] E. Bard, C.R. Geoscience 336 (2004) 603–638.
[3] J. Croll, Climate and Time in Their Geological Relations: A Theory of Secular Changes of the Earth's Climate, 1875, Appleton, New York, 577 pp.
[4] M. Milankovitch, Kanon der Erdbestrahlung und seine Anwendung auf des Eiszeitenproblem, Royal Serbian Sciences, Spec. Publ. 132, section of Mathematical and natural Sciences, vol. 33, 1941, Belgrade, 633 pp.
[5] A.L. Berger, Long-term variations of daily insolation and quaternary climatic change, J. Atmos. Sci. 35 (1978) 2362–2367.
[6] J. Imbrie, J.D. Hays, D.G. Martinson, A. McIntyre, A.C. Mix, J.J. Morley, N.G. Pisias, W.L. Prell, N.J. Shackleton, The orbital theory of Pleistocene climate: support from a revised chronology of the marine delta 18O record, in: A. Berger, J. Imbrie, J. Hays, G. Kukla, B. Saltzman (Eds.), Milankovitch and Climate, Part I, Reidel Publishing Co., Boston, 1984, pp. 269–305.
[7] M.J. Suarez, I.M. Held, The sensitivity of an energy balance climate modele to variations in the orbital parameters, J. Geophys. Res. 84 (1979) 4825–4836.
[8] J. Imbrie, J.Z. Imbrie, Modelling the climatic response to orbital variations, Science 207 (1980) 943–953.
[9] D. Rind, D. Petteet, G. Kukla, Can Milankovitch orbital variations initiate the growth of ice sheets in a general circulation model? J. Geophys. Res. (Atmosphere) 94 (1989) 12851–12871.
[10] A. Berger, H. Gallee, C. Tricot, Glaciation and deglaciation mechanisms in a coupled two-dimensional climate–ice-sheet model, J. Glaciol. 39 (1993) 45–49.
[11] B. Dong, P. Valdes, Sensitivity studies of northern hemisphere glaciation using an atmospheric general circulation model, J. Clim. 8 (1995) 2471–2495.
[12] N. de Noblet, I.C. Prentice, S. Joussaume, et al., Possible role of atmosphere–biosphere interactions in triggering the last glaciation, Geophys. Res. Lett. 23 (1996) 3191–3194.
[13] M. Khodri, Y. Leclainche, G. Ramstein, et al., Simulating the amplification of orbital forcing by ocean feedbacks in the last glaciation, Nature 410 (2001) 570–574.
[14] M. Khodri, G. Ramstein, N. De Noblet, M. Kageyama, Sensitivity of the northern extratropics hydrological cycle to the changing insolation forcing at 126 and 115 ky BP, Clim. Dyn. 21 (3–4) (2003) 273–287.
[15] M. Khodri, G. Ramstein, D. Paillard, J.C. Duplessy, M. Kageyama, A. Ganopolsky, Modelling the climate evolution from the last interglacial climate to the start of the last glaciation: the role of Arctic Ocean freshwater budget, Geophys. Res. Lett. 30 (12) (2003) (8)1–(8)4 (1606).
[16] Z. Wang, L.A. Mysak, Simulation of the last glacial inception and rapid ice sheet growth in the McGill Paleoclimate Model, Geophys. Res. Lett. 29 (23) (2002), doi:10.1029/2002GL015120 (2102).
[17] M. Crucifix, M.-F. Loutre, Transient simulations over the last interglacial period (126–115 kyr BP): feedback and forcing analysis, Clim. Dyn. 19 (2002) 417–433.
[18] G. Vettoretti, W.R. Peltier, Post-Eemian glacial inception: Part I. The impact of summer seasonal temperature bias, J. Clim. 16 (2003) 889–911.
[19] G. Vettoretti, W.R. Peltier, Post-Eemian glacial inception: Part II. Elements of a cryospheric pump, J. Clim. 16 (2003) 912–927.
[20] G. Vettoretti, W.R. Peltier, Sensitivity of glacial inception to orbital and greenhouse gas climate forcing, Quat. Sci. Rev. 23 (2004) 499–519.

[21] J.F. Royer, M. Déqué, P. Pestiaux, Orbital forcing of the inception of the Laurentide ice sheet? Nature 304 (1983) 43–46.
[22] G. Kukla, J. Gavin, Milankovitch climate reinforcements, Glob. Planet. Change 40 (1–2) (2004) 27–48.
[23] E. Cortijo, S. Lehman, L. Keigwin, et al., Changes in meridional temperature and salinity gradients in the North Atlantic Ocean (30° to 72°N) during the last interglacial period, Paleoceanography 14 (1) (1999) 23–33.
[24] M.R. Chapman, N.J Shackleton, Global ice-volume fluctuations, North Atlantic ice rafting events, and deep-ocean circulation changes between 130 and 70 ka, Geology 27 (1999) 795–798.
[25] M.R. Chapman, N.J. Shackleton, Millennial-scale fluctuations in North Atlantic heat flux during the last 150,000 years, Earth Planet. Sci. Lett. 159 (1998) 57–70.
[26] N.J. Shackleton, M. Chapman, M.F. Sánchez Goñi, D. Pailler, Y. Lancelot, The classic marine isotope substage 5e, Quat. Res. 58 (2002) 14–16.
[27] M.F. Sánchez Goñi, F. Eynaud, J.L. Turon, N.J. Shackleton, High resolution palynological record off the Iberian margin: direct land–sea correlation for the last interglacial complex, Earth Planet, Sci. Lett. 171 (1999) 123–137.
[28] P.C. Tzedakis, M.R. Frogley, T.H. Heaton, Duration of the last interglacial conditions in northwestern Greece, Quat. Res. 58 (2002) 53–55.
[29] W.L. Prell, J.E. Kutzbach, Monsoon variability over the past 150,000 years, J. Geophys. Res. 92 (D7) (1987) 8411–8425.
[30] R.G. Gallimore, J.E. Kutzbach, Role of orbitally induced changes in tundra area in the onset of glaciation, Nature 381 (1996) 503–505.
[31] A.C. Clement, A. Hall, A.J. Broccoli, The importance of precessional signals in the tropical climate, Clim. Dyn. 22 (2004) 327–341.
[32] P. Braconnot, O. Marti, Impact of precession on monsoon characteristics from coupled ocean atmosphere experiments: changes in Indian monsoon and Indian ocean climatology, Mar. Geol. 201 (2003) 23–34.
[33] S.C. Jackson, A.J. Broccoli, Orbital forcing of Arctic climate: mechanisms of climate response and implications for continental glaciation, Clim. Dyn. 21 (2003) 539–557.
[34] Y. Le Clainche, P. Braconnot, O. Marti, S. Joussaume, J.-L. Dufresne, M.-A. Filiberty, The Role of Sea Ice Thermodynamics in the Northern Hemisphere Climate Simulated by the Coupled Ocean–Atmosphere–Sea Ice Model, Note du Pôle de modélisation, Institut Pierre-Simon Laplace, 2001, Available online at http://www.ipsl.jussieu.fr/poles/Modelisation/NotesScience/note21.pdf.
[35] P. Braconnot, O. Marti, S. Joussaume, Y. Leclainche, Ocean feedback in response to 6 kyr BP insolation, Clim. Dyn. 13 (2000) 1537–1553.
[36] N. Ducoudré, K. Laval, A. Perrier, SECHIBA, a new set of parameterisations of the hydrologic exchanges at the land–atmosphere interface within the LMD atmospheric general circulation model, J. Clim. 6 (1993) 248–273.
[37] M.-A. Filiberti, J.-L. Dufresne, J.-Y. Grandpeix, Reference Manual for IGLOO Sea Ice Mode, Note Technique du Pôle de Modélisation, Institut Pierre-Simon Laplace, 2001, 35pp.
[38] J.-L. Dufresne, P. Friedlingstein, M. Berthelot, L. Bopp, P. Ciais, L. Fairhead, H. Le Treut, P. Monfray, On the magnitude of positive feedback between future climate change and the carbone cycle, Geophys. Res. Lett. 29 (1405) (2002), doi:10.1029/2001GL013777.
[39] P. Braconnot, Tests de sensibilité avec le modèle d'atmosphère du LMD en vue d'améliorer le couplage avec l'océan, Institut Pierre-Simon Laplace, 1998, (Note 2, 39 pp. [Available online at: www.ipsl.jussieu.fr/modélisation/liste-notes-tech.html).
[40] D.R. Legates, C.J. Willmott, Monthly average surface air temperature and precipitation. Digital raster data on a 30 minute Cartesian orthonormal geodetic (lat/long) 360 × 720 grid. In: Global Ecosystems Database Version 2.0. Boulder, CO: NOAA National Geophysical Data Center (1992). Forty-eight independent and four derived single-attribute spatial layers. 47,846,439 bytes in 194 files. [first published in 1989].
[41] W.J. Schmitz, M.S. McCartney, On the North Atlantic circulation, Rev. Geophys. 31 (1993) 29–49.
[42] R. Seager, D.S. Battisti, J. Yin, N. Gordon, N. Naik, A.C. Clement, M.A. Cane, Is the Gulf Stream responsible for Europe's mild winters? Quart. J. Roy. Meteor. Soc. 128 (586) (2002) 2563–2586 (Part B).
[43] E. Cortijo, J.C. Duplessy, L. Labeyrie, H. Leclaire, J. Duprat, T.C.E van Weering, Eemian cooling in the Norwegian Sea and North Atlantic ocean preceding continental ice-sheet growth, Nature 372 (1994) 446–449.
[44] J.F. Adkins, E.A. Boyle, L. Keigwin, E. Cortijo, Variability of the North Atlantic thermohaline circulation during the last interglacial period, Nature 390 (1997) 154–156.
[45] I.R. Hall, N. McCave, M.R. Chapman, N.J. Shackleton, Coherent deep flow variation in the Iceland and American basins during the last interglacial, Earth Planet. Sci. Lett. 164 (1998) 15–21.
[46] R. Lee, B. Barkstrom, Characterization of the earth radiation budget experiment radiometers, Metrologia 28 (1991) 183–187.
[47] E. Kalnay, M. Kanamitsu, R. Kistler, W. Collins, D. Deaven, L. Gandin, M. Iredell, S. Saha, G. White, J. Woollen, Y. Zhu, M. Chelliah, W. Ebisuzaki, J.W. Higgins, K. Janowiak, C. Mo, C. Ropelewski, J. Wang, A. Leetmaa, R. Reynolds, R. Jenne, D. Joseph, The NCEP/NCAR 40-year reanalysis project, Bull. Am. Meteorol. Soc. 77 (1996) 437–471.